MALDI Ionization Mechanisms Investigated by Comparison of Isomers of Dihydroxybenzoic Acid

Kristopher M. Kirmess[†], Richard Knochenmuss[‡*], Gary J. Blanchard[**], Gary R. Kinsel[†]

[†] Department of Chemistry and Biochemistry, Southern Illinois University at Carbondale, Carbondale, IL. 62901

[‡] RKResearch, Seftigen, Switzerland

[**] Department of Chemistry, Michigan State University, East Lansing, MI. 48824

Published as J. Mass Spectrom. 2016, 51, 79–85, DOI 10.1002/jms.3725

Abstract

Matrix-assisted laser desorption/ionization (MALDI) ion formation mechanisms were investigated by comparison of isomers of dihydroxybenzoic acid. These exhibit substantially different MALDI performance, the basis for which was not previously understood. Luminescence decay curves are used here to estimate excited electronic state properties relevant for the Coupled Chemical and Physical Dynamics (CPCD) model. With these estimates, the CPCD predictions for relative total ion and analyte ion yields are in good agreement with the data for the DHB isomers. Predictions of a thermal equilibrium model were also compared and found to be incompatible with the data.

* Author for correspondence

Introduction

Since it's introduction in 1990, one of the more commonly used MALDI matrices has been 2,5 dihydroxybenzoic acid (2,5 DHB).[1] Six positional isomers of dihydroxybenzoic acid exist, but only 2,5 DHB has achieved wide acceptance (sometimes mixed with the closely related 2-hydroxy, 5-methoxybenzoic acid as "super DHB".[2]) This preference reflects the fact that DHB isomers exhibit significantly varying MALDI performance. Understanding these differences could help clarify fundamental mechanisms underlying the MALDI method. The DHB isomers are particularly attractive in this context because 2,5 DHB is probably the most extensively studied matrix of all. Wide-ranging reference information is therefore available.

There have been a few earlier comparisons of DHB isomers. Jessome et al.[3] compared their MALDI performance for a variety of analytes including peptides, proteins, oligonucleotides and polysaccharides. The 2,3 2,5 and 2,6 isomers all gave useful results, though relative rankings varied with analyte class. No correlation with ionization potential, proton affinity or solution absorption cross section was found.

Performance with the polyethylene glycols was investigated by Lee et al.[4], using solvent free and conventional preparations. For these synthetic polymers, the 2,6 isomer was best, but 2,3 and 2,5 also performed well. The other isomers were considered unusable.

The melting points and enthalpies of sublimation were determined by Price, Bashir and Derrick.[5] Once again, no correlation between these parameters and MALDI performance could be established.

A variety of primary ionization mechanisms have been proposed, see reference 6 for a review. In the case of 2,5 DHB evidence such as fluorescence quenching and trapping by dopants strongly suggests that mobile electronic excitations (excitons) play a key role. Pooling of these excitons allows concentration of sufficient energy for initial charge separation. A detailed, quantitative model has been constructed for 2,5 DHB and other matrices, in which the photochemistry and ablation physics are coupled to predict the final

ion yield of both matrix and analyte.[7-11] Primary matrix ionization is followed by secondary charge transfer reactions with analytes. This Coupled Chemical and Physical Dynamics (CPCD) model has successfully reproduced a number of MALDI phenomena observed with 2,5 DHB and other matrices such as alpha-4-hydroxycyanocinnamic acid (CHCA),[12] 4-chloro-α-cyanocinnamic acid[12] and 2,4,6 trihydroxyacetophenone (THAP)[13]. In addition to those listed in reference [6], recent successful results have included bipolar ion ratios as a function of secondary reaction energetics,[9] yields vs. wavelength and fluence of three matrices,[14] explanation of a set of phenomena in "temperature-selected" spectra,[15] and absolute ion yields vs fluence in two matrices.[12]

In light of the CPCD success with the 2,5 isomer, a natural question is whether or not other DHB isomers exhibit exciton pooling, and whether this is correlated with MALDI performance. These questions are not restricted to singlet excited states. As was recently shown for THAP matrix, and as is typical for aromatic ketones, intersystem crossing to triplets may be quite efficient,[13] from which a variety of reaction pathways are known, including formation of ionic products.[16] Intersystem crossing may also be affected by external heavy atoms, such as halogen anions in salt impurities, which may be abundant in commercial matrix.

All the 2,X DHB isomers include the salicylic acid intermolecular hydrogen bonding motif, between the carboxylic acid and the 2-OH group. By analogy to salicylic acid, intramolecular excited state proton transfer (ESPT) has been suggested as a primary charge transfer step.[17-24] The 3,X isomers obviously do not have this motif, making them an interesting control group. However, ESPT is known to be very dependent on a strongly solvating environment for ions, which is not the case in the solid matrix nor in the early MALDI plume.[25] Also, evidence for ESPT has been sought in 2,5 DHB, but was not found.[26, 27]

Models which do not include electronic excitations as a necessary factor can be separated into two subgroups: direct and indirect thermal processes. The direct mechanisms

consider the effect of high temperature in the plume on charge transfer (e.g. proton transfer) reaction equilibria. As temperature increases, the degree to which energetic processes such as charge transfer proceed increases. The dense ablated matrix material might act as a solvent, further favoring charge separation. This is the Polar Fluid Model (PFM), which was proposed early in the study of MALDI mechanisms,[28, 29] but was only recently quantitatively explicated by the Ni group.[30] Similar thermal proposals were made by the Kim group.[31, 32] These proposals are based on recent attempts to measure ion yields,[33-38] which were interpreted as being inconsistent with non-thermal models.

Assumptions of the PFM have been challenged, with the consequence that yields are likely many orders of magnitude lower than observed.[25] In addition, other MALDI observations used to argue for a thermal model[31] have been shown to be completely consistent with the CPCD.[15]

Indirect thermal models require thermal (or other) energy to break the sample apart, which initiates another charge separation mechanism. The best known is the Lucky Survivors model, in which preformed ions are assumed to exist in the sample before irradiation, and are simply liberated.[39, 40] Also in this category is the pneumatic assistance model[41] which is based on bursting bubbles of matrix vapor.[42] This bears some similarity to recent proposals for mechanisms of "inlet" ionization, which also invoke physical disintegration as a key step.[43]

Here we examine properties of the DHB isomers in the context of possible thermal and non-thermal MALDI ionization mechanisms. While not generalizable to all MALDI matrix materials, the results shed light on MALDI performance of this group of matrices, and especially the widely used 2,5 isomer.

Experimental

The MALDI matrices 2,3-dihydroxybenzoic acid (2,3-DHB), 2,4-dihydroxybenzoic acid (2,4-DHB), 2,5-dihydroxybenzoic acid (2,5-DHB), 2,6-dihydroxybenzoic acid (2,6-DHB), 3,4-

dihydroxybenzoic acid (3,4-DHB), and 3,5-dihydroxybenzoic acid (3,5-DHB) were purchases from Sigma-Aldrich (St. Louis, MO.) HPLC grade acetonitrile and polyethylene glycol (PEG) (average M_n 950-1050 Da) were also purchased from Sigma-Aldrich (St. Louis, MO.) Human angiotensin II was purchased from Bio-Rad Laboratories (Hercules, CA.)

Purification of MALDI Matrices

Thin films of the MALDI matrices were created by subliming the matrices onto pre-cleaned aluminum substrates. 100 mg of the particular matrix was placed at the bottom of the sublimation chamber and the substrate was affixed to the bottom of the chamber via vacuum adhesive tabs. Cold water (10^{o} C) was circulated through the cold finger after 5 minutes under reduced pressure (0.1 Torr). Heat was then applied to the base of the chamber by means of a sand bath. The temperature of the sand bath was monitored throughout the sublimation and maintained below the melting point of the respective sample. After 20 minutes, the chamber was removed from the heat source and was maintained under vacuum for an additional ten minutes after which the chamber was vented to atmosphere. The resultant thin films appeared to be uniform but were not further characterized. Excess sublimed matrix was scrapped from the bottom of the cold finger, collected, and used later in MALDI-MS experiments.

MALDI-MS

Purified MALDI matrices were dissolved in an acetonitrile/water mixture (2:1 v/v) to yield final concentrations of 10 mg/mL. Human angiotensin II and PEG were also dissolved in the same acetonitrile/water mixture. The concentrations of both human angiotensin II and PEG were 1.00×10^{-4} mg/mL. To the pre-cleaned 96 spot polished steel MALDI plate, 0.5 µL of each matrix solution was spotted and allowed to air dry. Once dry, 0.5 µL of the analyte solution was spotted onto each dried matrix spot and allowed to air dry for 30 minutes prior to analysis by MALDI-MS.

All mass spectra were acquired using a Bruker Microflex LR time-of-flight (TOF) mass spectrometer (Bruker Daltonics, Billerica, MA.). The instrument was operated in positive ion linear mode using pulsed extraction (18.75 kV acceleration). Laser desorption was

performed using a nitrogen laser (337 nm). The ion extraction delay was set to 100 ns while spectra of 100 laser shots were summed and recorded for each matrix.

Luminescence Decay Curves

Fluorescence lifetime measurements were performed using a time-correlated single photon counting (TCSPC) instrument that has been described in detail previously.[44] Briefly, the light source is a CW passively mode-locked Nd:YVO_4 laser (Spectra Physics Vanguard) that produces 2.5 W average power at both 355 nm and 532 nm, with 13 ps pulses at 80 MHz repetition rate. The 355 nm output of the source laser is used to excite a cavity-dumped dye laser (Coherent 702) operating at 674 nm with Sulforhodamine 640 dye (Exciton) and producing 5 ps pulses at a repetition rate of 4 MHz (Gooch and Housego cavity dumping electronics). Pulses from the dye laser are divided into excitation and reference arms, with the reference channel being detected by a photodiode (Becker & Hickl PHD-400-N). The excitation pulse train is frequency doubled using a $LiIO_3$ Type I second harmonic generation crystal. The fundamental is separated from the second harmonic with a BG-3 color filter (transmittance <0.01 at the fundamental, >0.98 at the harmonic) and the second harmonic polarization is rotated to vertical using a quartz rhomb pair. The 337 nm average power at the sample was *ca*. 1 mW and the beam focused to a 10 μm diameter spot. This resulted in a fluence per shot of approximately 0.3 mJ/cm^2.

Emission is collected using a 40x reflecting microscope objective (Ealing) and the components polarized parallel (0°) and perpendicular (90°) with respect to the vertically polarized excitation pulse are separated using a polarizing cube beam splitter. The polarized signal components are detected simultaneously using two microchannel plate photomultipliers (MCP-PMT, Hamamatsu R3809U-50), after passing through subtractive double monochromators (Spectral Products CM-112).

The detection electronics (Becker & Hickl SPC-132) produce a *ca*. 40 ps response function for each detection channel. Data acquisition, detector bias, collection wavelength and time window are all controlled using a program written in-house in LabVIEW® (National Instruments).

The instrument is equipped to measure emission anisotropy, but the highly structured microcrystalline samples investigated here unfortunately lead to highly variable and poorly reproducible polarization ratios. All decay transients reported here are therefore unpolarized.

Multiple decay curves were acquired on multiple locations of the samples. As a typical example, three repetitions at three locations for a total of nine decay curves. Both the replicates at a location and the measurements at different locations were highly consistent, to within the experimental uncertainty.

Results and Discussion

Matrix excited state dynamics and the CPCD non-thermal model

Non-thermal models such as the CPCD invoke electronic excited states as the key intermediates in ultraviolet MALDI primary ion formation. In the CPCD, matrix excitons are the key to primary ion formation. In 2,5 DHB, 2,6 DHB, cinnamic acid, CHCA, ferulic acid, SA, ABA and 3-hydroxy picolinic acid.[45-51] singlet excitons have been shown to be mobile and undergo so-called annihilation reactions with each other. These reactions concentrate energy and are proposed to be responsible for initial charge separation.

As developed for 2,5 DHB, the relevant excited state pooling reactions are:

$S_0 + h\varpi \rightarrow S_1$ Matrix photoexcitation

$S_1 + S_1 \rightarrow S_n + S_0$ Pooling of two S_1 excitons

$S_n + S_1 \rightarrow$ Matrix ion pair + S_0 Pooling including one higher excited state.

The process requires a total of three photons. The ion pair is not specified in the CPCD, it must only be energetically less than or equal to the sum of the energies of the final pooling excitons. Electron transfer, $M^+ + M^-$, and proton transfer, $MH^+ + (M\text{-}H)^-$, pairs are the main possibilities. The former is considered most likely, with the latter a subsequent product, but the CPCD only assumes that all primary ions are matrix ions, analyte ions are created by ion-molecule secondary reactions.

As shown for THAP,[13] in some matrices, strong intersystem crossing may mean that triplet-triplet reactions are instead the main ionization pathway. That is not believed to be the case for the DHB isomers, and triplet pooling is assumed to play no role here.

Since singlet pooling has been repeatedly verified in 2,5 DHB by fluence-dependent fluorescence quenching, we proceed here with the working hypothesis that it also takes place in the other DHB isomers. To estimate the magnitude of the effect, luminescence decay curves are used. The intermolecular interactions in the solid state that lead to pooling are also a nonradiative internal conversion channel. Assuming this channel is

faster than the radiative emission rate and is the dominant nonradiative channel, the inverse of the lifetime can be used as a proxy for the pooling rate. This hypothesis has the advantage that high excitation fluences are not necessary to estimate the relative strength of pooling in DHB isomers. An example decay curve is shown in Figure 1, the others are shown in the supplementary material.

Figure 1 here

The S_1 lifetime corresponds to the initial decay rate immediately after excitation. The second, slow decay component at longer time is presumed to be a triplet. S_1 decay, intersystem crossing and the triplet decay were simultaneously fit to the decay curves. For the CPCD calculations below, the S_1 lifetime is the key parameter, and is shown in Table 1, along with the proposed relative pooling strength derived from it. The latter is defined as 1/(S_1 lifetime) normalized to the value of the 2,5 isomer.

Table 1 here

The 2,5 isomer was chosen as the reference because it has been investigated in detail. The rates are taken here from reference 14: S_1+S_1 pooling, $7x10^9$ s^{-1}, and S1+S_n pooling $1x10^9$ s^{-1}. The S_1+S_1 pooling rate constant was well constrained by the experimental data in that study, which covered a range of excitation densities. The S_1+S_n pooling rate constant is more difficult to establish, since its' most apparent effect is in the absolute yield, which is difficult to measure accurately. Recent results suggest that the value used here may be high, but scaling it downward to $3x10^6$ s^{-1} for agreement with absolute yield data was found to have no effect on relative comparisons similar to those presented here.[12]

The remaining factor needed for the CPCD calculation is the absorption cross section of each isomer in the solid state. This is important because it determines the density of excitations, and hence has a strong effect on pooling efficiency. Relative cross sections are sufficient, since the 2,5 isomer can again be used as reference. These were obtained from

thin film spectra, as described in the supplementary material, and are listed in Table 2.

Table 2 here

With the above information the CPCD can now be applied. The working hypothesis is that the relative pooling rate constants can be inferred from the low fluence nonradiative relaxation rates, because they are two consequences of the same intermolecular interactions. The relative experimental and CPCD total ion yields for the six DHB isomers are shown in Fig. 2. The zigzag pattern observed in the data is reproduced in the calculations, and agreement with the angiotensin TIY data is excellent. The PEG TIY data show less modulation but the pattern is the same.

Figure 2 here

Comparative CPCD results for the angiotensin yields (including molecular ions and fragments) are shown in Fig. 3 These calculations required a further input, the secondary charge transfer reaction free energy. In the CPCD model, matrix primary ions react with analyte neutrals to form the observed analyte ions in the case of angiotensin proton adducts. The reaction energy was therefore taken to be the difference between the gas phase basicities of the analyte and the corresponding matrices. The matrix data are shown in supplementary table S1. The angiotensin basicity is not known, so a reference reaction energy of -150 kJ/mol with the 2,5 isomer was used, and the others adapted according to table S1. The relative yields, normalized to the 2,3 isomer, were found to be insensitive to the reference reaction energy.

Once again, good, if not exact, agreement with the data is found. The 2,4 and 3,5 isomers lie outside the error bars, but the trend across the isomers is correct. It should be noted that factors which are not needed for the TIY comparison are relevant here, such as matrix-analyte reaction kinetics and analyte incorporation into the solid matrix. The variability of these with isomer has not been investigated.

No CPCD calculation was carried out for the PEG analyte because the amounts of sodium and potassium in the sample are not known. Multiple reactions with the analyte (in this case H^+, Na^+ and K^+ transfer) are also currently not included in the CPCD. At the same time, it is evident that the summed PEG signal follows the same general pattern as

angiotensin, though the differences between matrices are larger.

Figure 3 here

Comparison of yields with thermal equilibrium primary ionization

Ion yields in thermal equilibrium models are based on the relation between the free energy of reaction and the equilibrium constant:

$K=\exp(-\Delta G/RT)$

The reaction in question is matrix autoprotolysis:

$2M \rightarrow MH^+ + (M-H)^-$

In the gas phase, this is less energetic than creation of a radical cation/anion pair. Ionization energies are above 775 kJ/mol (8 eV),[26, 52] and electron affinities below 50 kJ/mol,[53] so the electron transfer reaction energy is at least 725 kJ/mol. This is at least 150 kJ/mol higher than autoprotolysis, as seen in Table S1. In the dense early MALDI plume these values will be modified somewhat by solvation effects. The autoprotolysis equilibrium constant is:

$K=[MH^+][(M-H)^-]/[M^2] = X^2/(1-2X)^2$

Proponents of the thermal model argue that the fractional ion yield, X, is low, on the order of $1x10^{-8}$ for 2,5 DHB.[54] It is then reasonable to approximate the equilibrium constant as:

$K=X^2$

Note also that the ion to neutral ratio in each polarity also simplifies because X is small:

$X/(1-2X)\approx X$

The ratio of yields under otherwise identical conditions is then:

$(X_1/X_2)^2=K_1/K_2=\exp(-\Delta G_1/RT)/\exp(-\Delta G_2/RT)=\exp(-(\Delta G_1-\Delta G_2)/RT)$

$2 \ln(X_1/X_2) = -(\Delta G_1 - \Delta G_2)/RT$

$X_1/X_2 = \exp(-(\Delta G_1 - \Delta G_2)/2RT)$

This relation allows us to compare the TIY data with the thermal equilibrium model, by using one isomer as a reference, in this case 2,3 DHB. Fig. 4 shows this comparison, assuming that the average plume temperatures are the same in all cases.

Figure 4 here

Most striking is the prediction that the 2,6 isomer should be by far the most efficient matrix, which is not the case. Also the 3,x isomers are predicted to be much worse than observed.

The early plume is dense, possibly supercritical, and contains many clusters of various sizes, not all of which vaporize.[10, 11, 25] The energetics of autoprotolysis are not identical to the gas phase values throughout the ablation event. However, there is currently no reason to expect that the relative reaction energetics of the isomers will be significantly different in those environments than in the gas phase. The calculations in Fig. 4 are therefore believed to be a reasonable first estimate of relative ionization efficiencies in the thermal equilibrium model.

As part of the polar fluid model[28, 29] developed in reference 30, the autoprotolysis yield was proposed to be determined by equilibrium in liquid matrix, before vaporization. A method was also proposed for ab initio calculation of the dielectric constant of this liquid, which modifies the effective autoprotolysis energy. While this approach is open to question,[25] it was used here as a further variant or development of the thermal model. The calculated dielectric constants are shown in Table S2.

The different isomers will reach different peak temperatures. The relative yields in the case of unequal temperatures are:

$X_1/X_2 = \exp(-(\Delta G_1/RT_1 - \Delta G_2/RT_2))$

The peak temperature is taken here to be proportional to the amount of laser energy

deposited per volume, as described by the relative absorption cross sections of Table 2. (Since these molecules are isomers, their heat capacities will not differ substantially) Using this correction, the trace with diamond symbols in Fig. 5 is obtained.

As a second estimate of peak temperatures prior to ablation, the experimental melting points were used[5] (asterisk symbols). Surprisingly, these may be higher than the true ablation temperatures, since a high vapor pressure has been observed for 2,5 DHB starting at about 170 °C, well below the nominal melting point of 206 °C.[55] Several other matrices also exhibited high vapor pressure at low temperature.

Figure 5 here

As is evident, agreement with experiment is significantly reduced compared to the simpler thermal model. The range of relative yields now spans more than 9 orders of magnitude, far beyond the experimentally observed range.

Conclusions

The relative MALDI performance of the six isomers of DHB was used to evaluate the CPCD thermal equilibrium and PFM models of MALDI ionization. Relative comparisons eliminate major experimental difficulties in measurement of absolute yield, and can be performed on most instruments.

In order to apply the CPCD, relative pooling efficiencies for the isomers are required. The pooling rates were taken to be approximately inversely related to the solid state singlet lifetimes. This flows from the hypothesis that intermolecular interactions which are responsible for pooling also largely determine the nonradiative relaxation which is the dominant factor in the lifetime. The success of this approach here suggests that high fluence measurements are not always required to determine CPCD pooling parameters, which could significantly ease application of the model.

With this approximation, and taking into account relative solid state absorption cross sections, the CPCD model gives very good agreement with the total ion yield data for the six DHB isomers, and thereby appears to resolve a long standing conundrum. Prior work sought correlation of MALDI performance with single quantities such as ionization potential or thermochemical parameters. The present results show that it is necessary to take into account the interaction of multiple phenomena, as the CPCD was designed to do.

Agreement of the CPCD with the angiotensin data is not as good as with the total ion yield data, but still generally satisfactory. Differences are quantitative rather than qualitative. Given the lack of detailed kinetic information on secondary charge transfer reactions of the isomers, and the unknown degree of analyte incorporation or exclusion, this result suggests the secondary ionization part of the CPCD is also largely correct.

Both the simple thermal equilibrium model and the more complex PFM proposed by Chu et al. were found to give poor agreement with the data. The trends with isomer are qualitatively different, and quantitative differences are large. The full PFM predicts variations between the isomers of nine orders of magnitude, compared to the one-two orders observed.

Figures

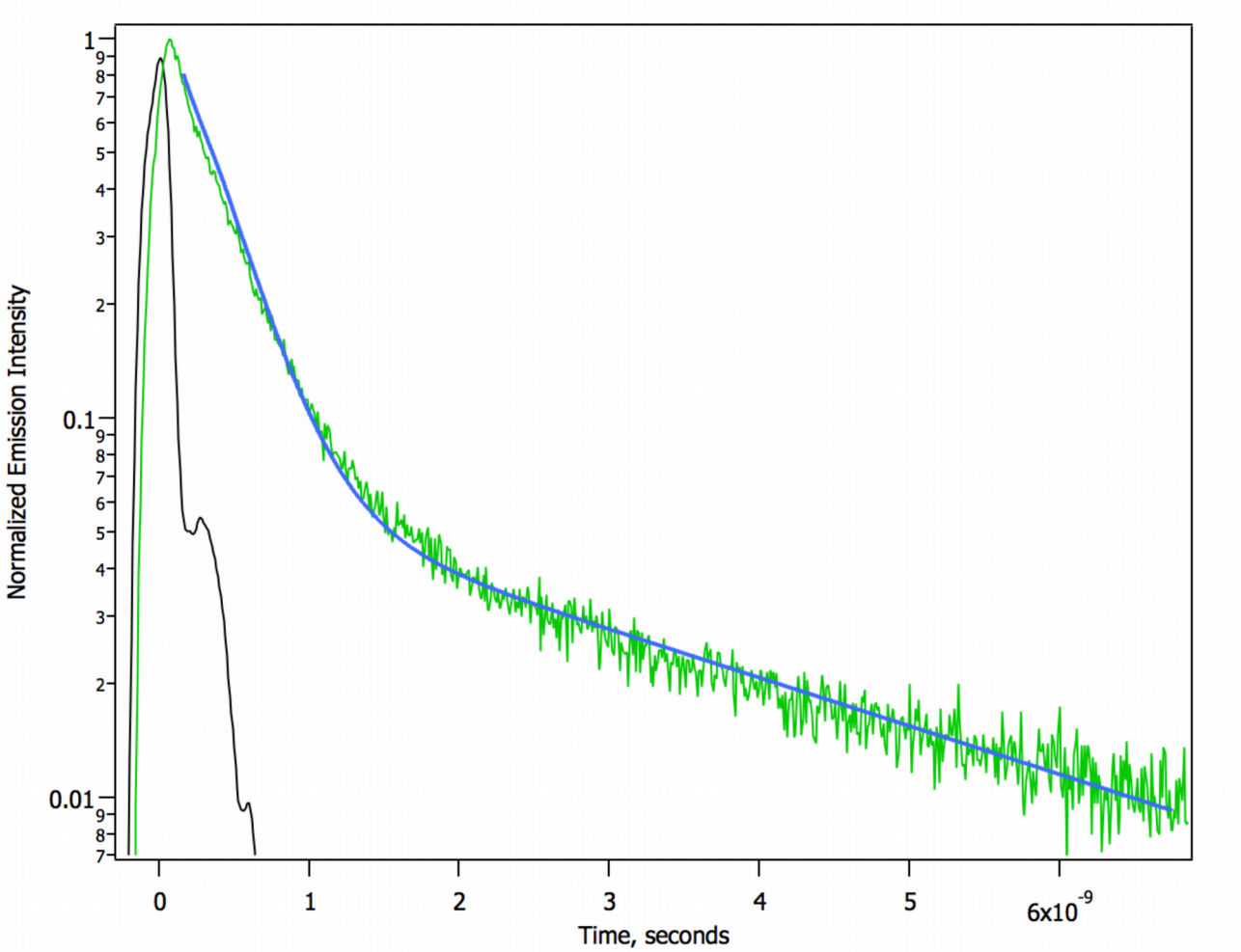

Figure 1. Time resolved emission of solid 3,4 dihydroxybenzoic acid. The CPCD fit to the data includes both singlet decay and intersystem crossing to a triplet. The sample was prepared by evaporation from THF solution. The measured instrument function is also shown. The resulting S_1 lifetime is 0.28 ns, and triplet lifetime 3.4 ns, Data and fits for the other isomers are shown in the supplementary material, and the S_1 lifetimes are listed in Table 1.

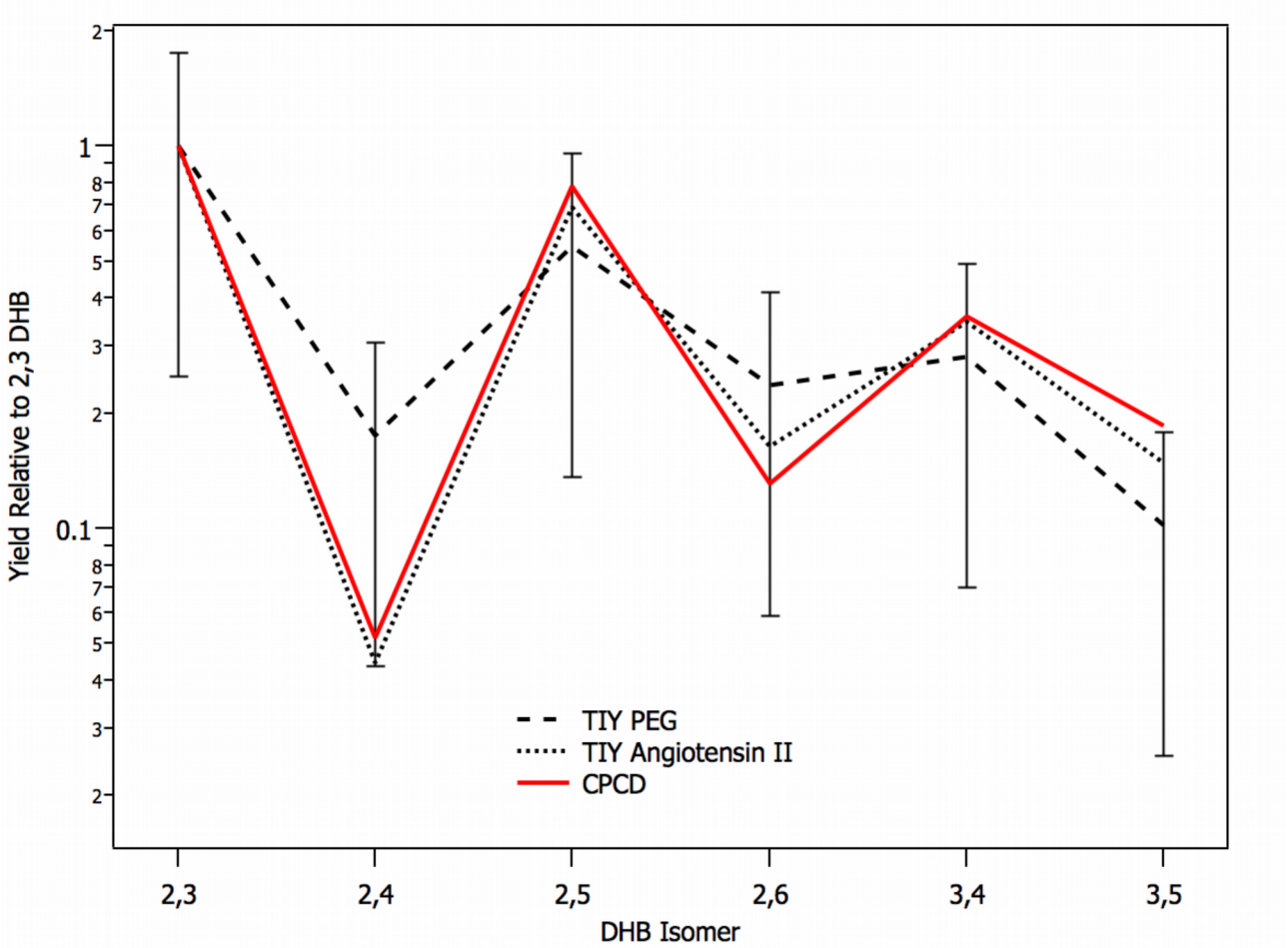

Figure 2. Total positive ion yields (ion/neutral ratio) for the six DHB isomers, scaled to the value of the 2,3 isomer. The points are connected with lines to guide the eye. The data for samples containing angiotensin II are indicated by a fine dashed line, the PEG-containing by a coarse dashed line. Error bars are shown for the PEG data, they are similar for the angiotensin data. The corresponding CPCD calculations are connected with a solid line.

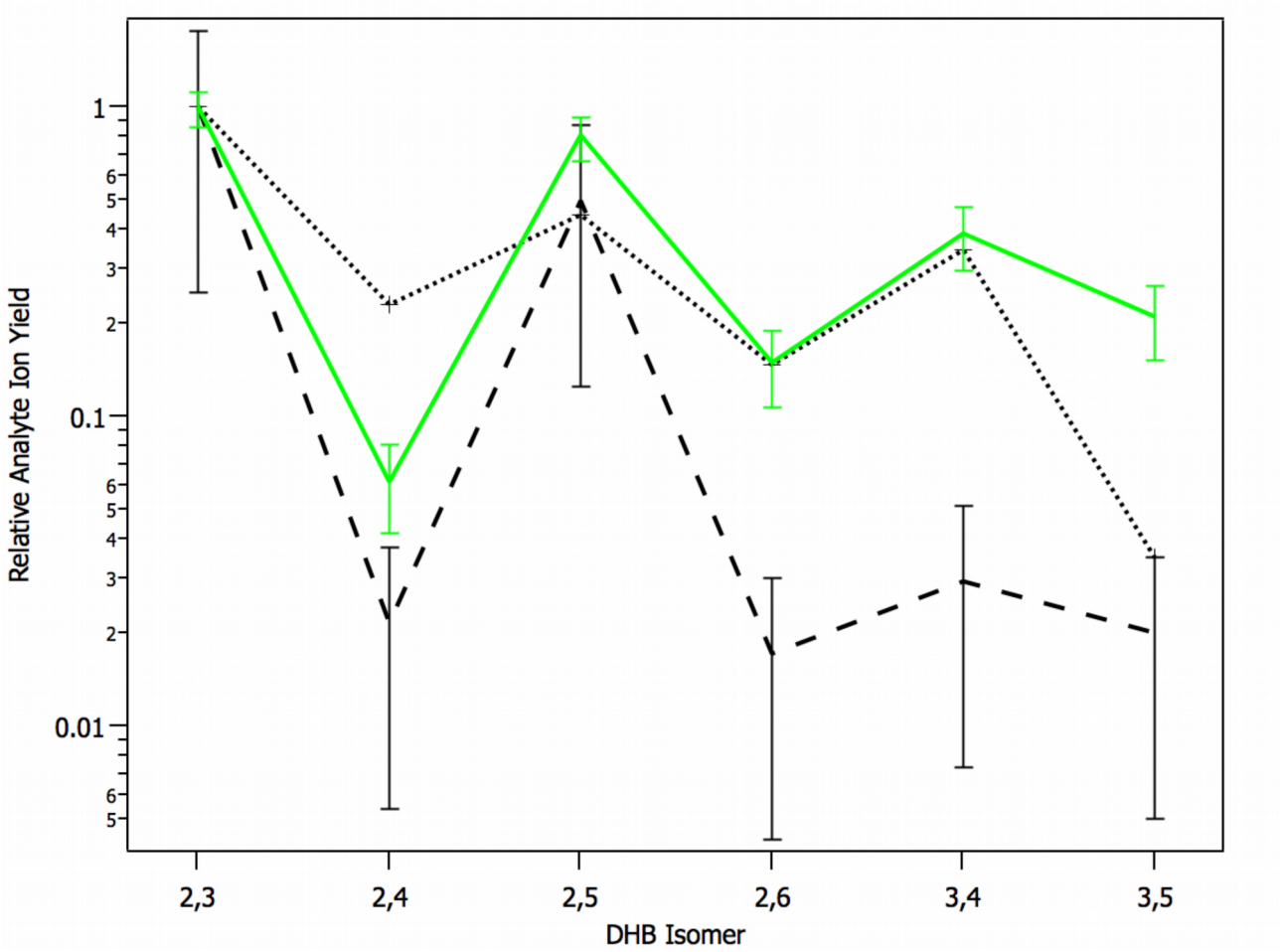

Figure 3. Total analyte positive ion yields (ion/neutral ratio) in all six DHB isomers. The data for samples containing angiotensin II are indicated by a fine dashed line, the PEG-containing by a coarse dashed line. In both cases, the data represent the sum of all analyte species, such as fragments in the case of angiotensin, and various cation adducts of all oligomers in the case of PEG. The corresponding CPCD calculations are connected with a solid line.

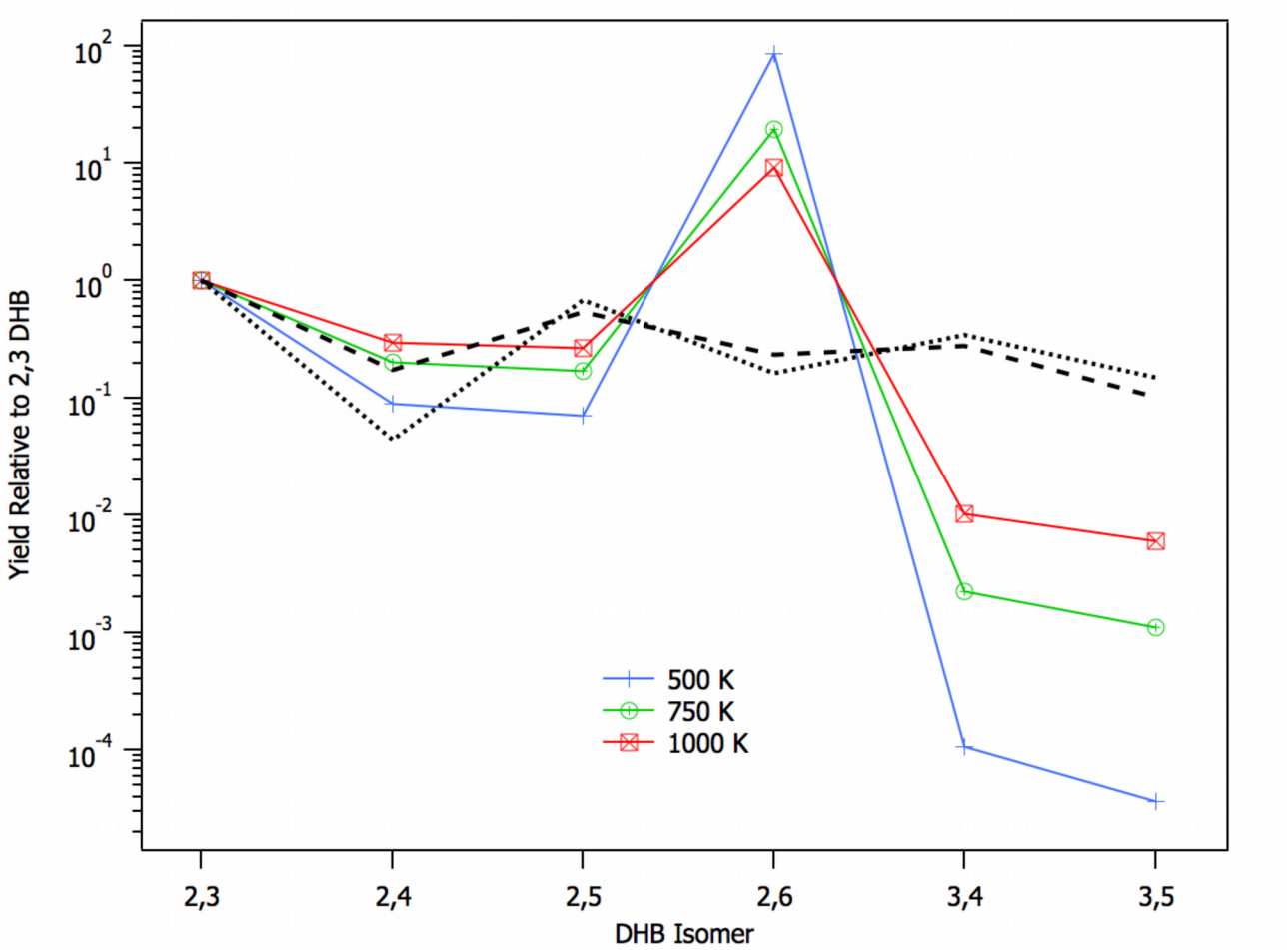

Figure 4. Relative total ion yields predicted by the simple thermal equilibrium autoprotolysis model, for all DHB isomers, and at three plume temperatures. The experimental TIY data of Fig. 2 is shown as dashed lines.

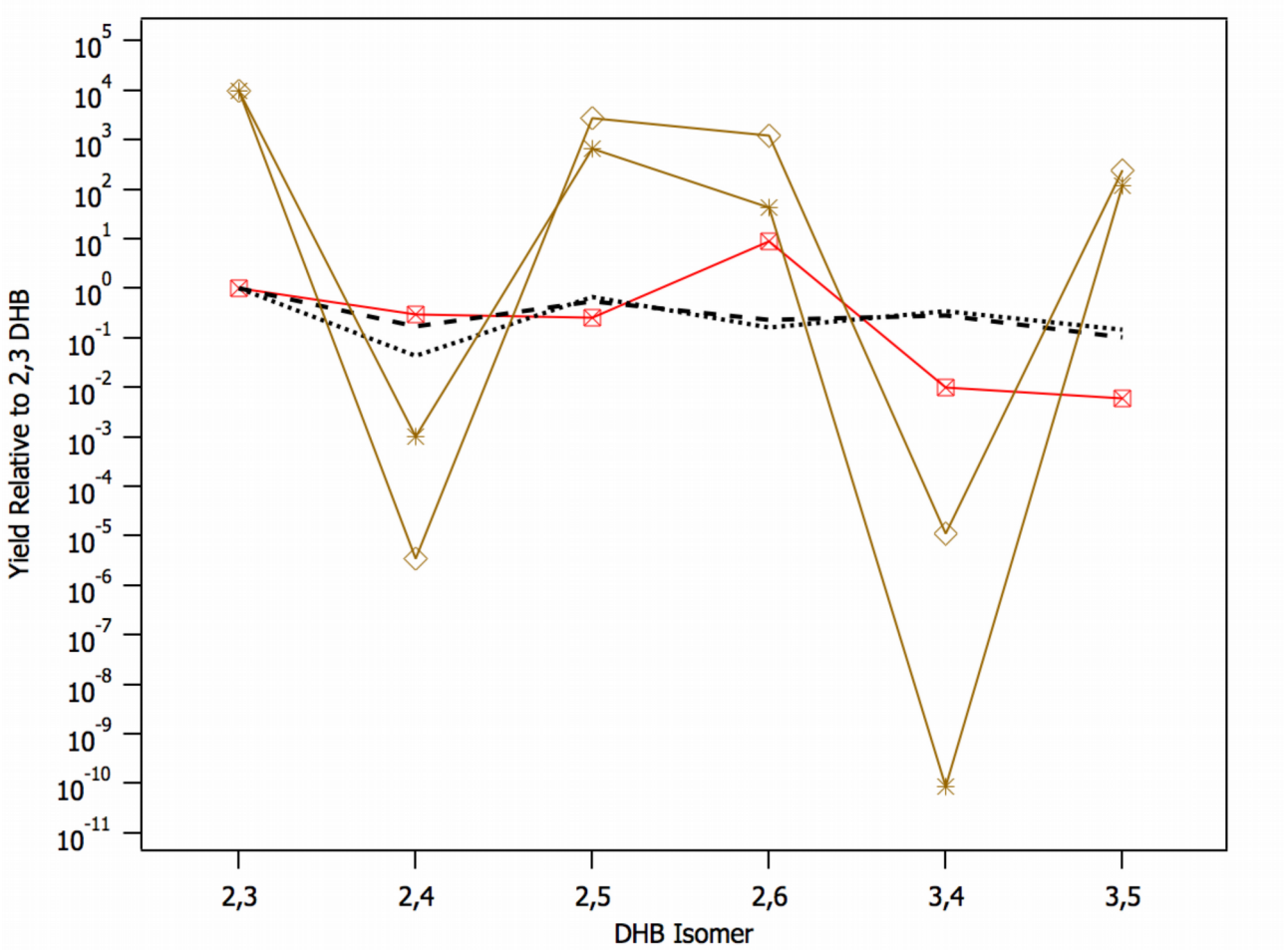

Figure 5. Full thermal PFM model as proposed by Chu et al.,[30] including ab initio dielectric constants. The equilibrium autoprotolysis model at a temperature of 1000 K is indicated by square symbols. The experimental data of Fig. 2 is indicated by dashed lines. Two temperature corrections are shown. The relative absorption cross section correction (diamonds) is based on Table 2. The melting point temperatures (asterisks) are based on the data of reference 5.

Tables

Table 1. Solid state singlet lifetimes of DHB isomers as fit to luminescence decay curves of samples prepared from THF. Typical experimental variability was approximately 25%. The relative pooling strength is defined here as 1/(S1 lifetime) normalized to the value of the 2,5 isomer.

Isomer	S_1 lifetime, ns	Relative pooling strength
2,3	0.12	1.8
2,4	0.80	0.28
2,5	0.22	1
2,6	1.7	0.13
3,4	0.28	0.79
3,5	2.0	0.11

Table 2. Estimated absorption cross sections of DHB isomers. The relative values were determined from thin film spectra, and scaled to the 2,5 isomer. The reference cross section of 2,5 DHB at 337 nm was taken to be 2×10^{-17} cm^2, as used in reference 14. See the supplementary material for data and further explanation.

Isomer	Absorption cross section relative to 2,5 DHB	Cross section, 10^{-17} cm^2
2,3	0.98	1.96
2,4	0.4	0.8
2,5	1	2.0
2,6	0.67	1.34
3,4	0.74	1.48
3,5	0.83	1.66

References

[1] K. Strupat, M. Karas, F. Hillenkamp. 2,5-dihydroxybenzoic acid: a new matrix for MALDI-MS. *Int. J. Mass Spectrom. ion Proc.* **1991,** *111,* 89.

[2] M. Karas, H. Ehring, E. Nordhoff, B. Stahl, K. Strupat, F. Hillenkamp, M. Grehl, B. Krebs. Matrix-Assisted Laser-Desorption/Ionization Mass-Spectrometry with Additives to 2,5-Dihydroxybenzoic Acid. *Org. Mass Spectrom.* **1993,** *28,* 1476.

[3] L. Jessome, N.-Y. Hsu, Y.-S. Wang, C.-H. Chen. Matrix-assisted laser desorption/ionization mechanism study with dihydroxbenzoic acid isomers as matrices. *Rapid Comm. Mass Spectrom.* **2008,** *22,* 130.

[4] A. Lee, H.-J. Yang, Y. Kim, J. Kim. Effect of Dihydroxybenzoic Acid Isomers on the Analysis of Polyethylene Glycols in MALDI-MS. *Bull. Korean Chem. Soc.* **2009,** *30,* 1127.

[5] D. M. Price, S. Bashir, P. R. Derrick. Sublimation properties of x,y-dihydroxybenzoic acid isomers as model MALDI matrices. *Thermochim. Acta* **1999,** *327,* 167.

[6] R. Knochenmuss. Ion formation mechanisms in UV-MALDI. *The Analyst* **2006,** *131,* 966.

[7] R. Knochenmuss. A Quantitative Model of Ultraviolet Matrix-assisted Laser Desorption and Ionization. *J. Mass Spectrom.* **2002,** *37,* 867.

[8] R. Knochenmuss. A Quantitative Model of UV-MALDI Including Analyte Ion Generation. *Anal. Chem.* **2003,** *75,* 2199.

[9] R. Knochenmuss. A bipolar rate equation model of MALDI primary and secondary ionization processes, with application to positive/negative analyte ion rations and suppression effects. *Int. J. Mass Spectrom.* **2009,** *285,* 105.

[10] R. Knochenmuss, L. V. Zhigilei. A molecular dynamics model of UV-MALDI including ionization processes. *J. Phys. Chem. B* **2005,** *109,* 22947.

[11] R. Knochenmuss, L. V. Zhigilei. Molecular dynamics simulations of MALDI: laser fluence and pulse width dependence of plume characteristics and consequences for matrix

and analyte ionization. *J. Mass Spectrom.* **2010,** *45,* 333.

[12] R. Knochenmuss. Ion Yields in the Coupled Chemical and Physical Dynamics Model of MALDI. *J. Am. Soc. Mass Spectrom.* **2015,** 26*,* 1645.

[13] K. M. Kirmess, R. Knochenmuss, G. J. Blanchard. Excited State Dynamics in the MALDI Matrix 2,4,6 Trihydroxyacetophenone: Evidence for Triplet Pooling Charge Separation Reactions. *Rapid Comm. Mass Spectrom.* **2014,** *28,* 2134.

[14] R. Knochenmuss. MALDI mechanisms: wavelength and matrix dependence of the coupled photophysical and chemical dynamics model. *The Analyst* **2014,** *139,* 147.

[15] R. Knochenmuss. MALDI Ionization Mechanisms: the Coupled Photophysical and Chemical Dynamics Model Correctly Predicts "Temperature"-Selected Spectra. *J. Mass Spectrom.* **2013,** *48,* 998.

[16] P. Jacques, X. Allonas, A. Sarbach, E. Haselbach, E. Vauthey. Tuning the ion formation process from triplet-triplet annihilation to triplet-mediated photoionization. *Chem. Phys. Lett.* **2003,** *378,* 185.

[17] M. Karas, D. Bachmann, U. Bahr, F. Hillenkamp. Matrix-Assisted Ultraviolet Laser Desorption of Non-Volatile Compounds. *Int. J. Mass Spectrom. Ion Proc.* **1987,** *78,* 53.

[18] M. E. Gimon, L. M. Preston, T. Solouki, M. A. White, D. H. Russell. Are Proton Transfer Reactions of Excited States Involved in UV Laser Desorption/Ionization? *Org. Mass Spectrom.* **1992,** *27,* 827.

[19] J. Krause, M. Stoeckli, U. P. Schlunegger. Studies on the Selection of New Matrices for Ultraviolet Matrix-Assisted Laser Desorption/Ionization Time-of-Flight Mass-Spectrometry. *Rapid Commun. Mass Spectrom.* **1996,** *10,* 1927.

[20] B. Spengler, R. Kaufmann. Gentle Probe for Tough Molecules: Matrix-Assisted Laser Desorption Mass Spectrometry. *Analusis* **1992,** *20,* 91.

[21] M. P. Chiarelli, A. G. Sharkey, D. M. Hercules. Excited-State Proton Transfer in Laser Mass Spectrometry. *Anal. Chem.* **1993,** *65,* 307.

[22] H. Yong. Photochemistry and Proton Transfer Reaction Chemistry of Selected

Cinnamic Acid Derivatives in Hydrogen Bonded Environments. *Int. J. Mass Spectrom. Ion Proc.* **1998,** *175,* 187.

[23] H.-C. Lüdemann, F. Hillenkamp, R. Redmond. Photoinduced Hydrogen Atom Transfer in Salicylate Acid Derivatives Used as Matrix-Assisted Laser Desorption/Ionization Matrices. *J. Phys. Chem. A* **2000,** *104,* 3884.

[24] K. Murakami, A. Sato, K. Hashimoto, T. Fujino. Study of ionization process of matrix molecules in matrix-assisted laser desorption ionization. *Chem. Phys.* **2013,** *419,* 37.

[25] R. Knochenmuss. Energetics and Kinetics of Thermal Ionization Models of MALDI. *J. Am. Soc. Mass Spectrom.* **2014,** *25,* 1521.

[26] V. Karbach, R. Knochenmuss. Do Single Matrix Molecules Generate Primary Ions in Ultraviolet Matrix-Assisted Laser Desorption/Ionization? *Rapid Commun. Mass Spectrom.* **1998,** *12,* 968.

[27] H. Fricke, K. Bartl, A. Funk, A. Gerlach, M. Gerhards. Proton/Hydrogen-Transfer Coordinate of 2,5-Dihydroxybenzoic Acid Investigated in a Supersonic Beam: Combined IR/UV Spectroscopy in the S_0, S_1 and D_0 States. *ChemPhysChem* **2008,** *9,* 2592.

[28] S. Niu, W. Zhang, B. T. Chait. Direct Comparison of Infrared and Ultraviolet Wavelength Matrix-Assisted Laser Desorption/Ionization Mass Spectrometry of Proteins. *J. Am. Soc. Mass Spectrom.* **1998,** *9,* 1.

[29] X. Chen, J. A. Carroll, R. C. Beavis. Near-Ultraviolet-Induced Matrix-Assisted Laser Desorption/Ionization as a Function of Wavelength. *J. Am. Soc. Mass Spectrom.* **1998,** *9,* 885.

[30] K. Y. Chu, S. Lee, M.-T. Tsai, I.-C. Lu, Y. A. Dyakov, Y. H. Lai, Y.-T. Lee, C.-K. Ni. Thermal Proton Transfer Reactions in Ultraviolet Matrix-Assisted Laser Desorption/Ionization. *J. Am. Soc. Mass Spectrom.* **2014,** *25*, 310.

[31] S. H. Ahn, K. M. Park, Y. J. Bae, M. S. Kim. Quantitative reproducibility of mass spectra in matrix-assisted laser desorption ionization and unraveling of the mechanism for gas-phase peptide ion formation. *J. Mass Spectrom.* **2013,** *48,* 299.

[32] Y. J. Bae, J. C. Choe, J. H. Moon, M. S. Kim. Why do the Abundances of Ions Generated by MALDI Look Thermally Determined? *J. Am. Soc. Mass Spectrom.* **2013,** *24,* 1807.

[33] Y. J. Bae, J. H. Moon, M. S. Kim. Expansion Cooling in the Matrix Plume is Under-Recognized in MALDI Mass Spectrometry. *J. Am. Soc. Mass Spectrom.* **2011,** *22,* 1070.

[34] Y. J. Bae, K. M. Park, M. S. Kim. Reproducibility of Temperature-Selected Mass Spectra in Mastrix-Assisted Laser Desorption Ionization of Peptides. *Anal. Chem.* **2012,** *84,* 7107.

[35] Y. J. Bae, Y. S. Shin, J. H. Moon, M. S. Kim. Degree of Ionization in MALDI of Peptides: Thermal Explanation for the Gas-Phase Ion Formation. *J. Am. Soc. Mass Spectrom.* **2012,** *23,* 1326.

[36] J. H. Moon, Y. S. Shin, Y. J. Bae, M. S. Kim. Ion Yields for Some Salts in MALDI: Mechanism for the Gas-Phase Ion Formation from Preformed Ions. *J. Am. Soc. Mass Spectrom.* **2011,** *23,* 162.

[37] J. H. Moon, S. H. Yoon, M. S. Kim. Temperature of Peptide Ions Generated by Matrix-Assisted Laser Desorption Ionization and Their Dissociation Kinetic Parameters. *J. Phys. Chem. B* **2009,** *113,* 2071.

[38] M.-T. Tsai, S. Lee, I.-C. Lu, K. Y. Chu, C.-W. Liang, C. H. Lee, Y. T. Lee, C.-K. Ni. Ion-to-neutral ratio of 2,5 dihydroxybenzoic acid in matrix-assisted laser desorption/ionization. *Rapid Comm. Mass Spectrom.* **2013,** *27,* 955.

[39] M. Karas, R. Krueger. Ion Formation in MALDI: the cluster ionization mechanism. *Chem. Rev.* **2003,** *103,* 427.

[40] M. Karas, M. Glückmann, J. Schäfer. Ionization in MALDI: singly charged molecular ions are the lucky survivors. *J. Mass Spectrom.* **2000,** *35,* 1.

[41] V. L. Talroze, R. L. Jacob, A. L. Burlingame, M. A. Baldwin. Insight into the MALDI mechanism: matrix decomposition and pneumatic assistance in plume formation. *Adv. Mass Sectrom.* **2001,** *15,* 481.

[42] L. Zilch, J. T. Maze, J. W. Smith, G. E. Ewing, M. F. Jarrold. Charge Separation in the Aerodynamic Breakup of Micrometer-Sized Water Droplets. *J. Phys. Chem. A* **2008,** *112,* 13352.

[43] S. Trimpin, B. Wang, E. D. Inutan, J. Li, C. B. Lietz, A. Harron, V. S. Pagnotti, D. Sardelis, C. N. McEwen. A Mechanism for Ionization of Nonvolatile Compounds in Mass Spectrometry: Considerations from MALDI and Inlet Ionization. *J. Am. Soc. Mass Spectrom.* **2012,** *23,* 1644.

[44] H. A. Pillman, G. J. Blanchard. Molecular Consequences of Ethanol Incorporation into Phospholipid Bilayers. *J. Phys. Chem. B* **2010,** *114,* 3840.

[45] H.-C. Lüdemann, R. W. Redmond, F. Hillenkamp. Singlet-singlet annihilation in ultraviolet MALDI studied by fluorescence spectroscopy. *Rapid Comm. Mass Spectrom.* **2002,** *16,* 1287.

[46] P. Setz, R. Knochenmuss. Exciton Mobility and Trapping in a UV-MALDI Matrix. *J. Phys. Chem. A* **2005,** *109,* 4030.

[47] T. Hoyer. Stationäre und zeitaufgelöste Photolumineszenz-Spektroskopie zur Analyse ultraschneller Photoreaktionen in MALDI- und Solarzellenproben. **2009,** *Dr. rer. nat.,* Carl von Ossietzky Universität Oldenburg, Oldenburg

[48] T. Hoyer, W. Tuszynski, C. Lienau. Ultrafast photodimerization dynamics in alpha-cyano-4-hydroxycinnamic and sinapinic acid crystals. *Chem. Phys. Lett.* **2007,** *443,* 107.

[49] T. Hoyer, W. Tuszynski, C. Lienau. Competing ultrafast photoinduced quenching reactions in cinnamic acid peptide blends. *Phys. Chem. Chem. Phys.* **2010,** *12,* 13052.

[50] H.-Y. Lin, H. C. Hsu, I.-C. Lu, K.-T. Hsu, C.-Y. Liao, Y.-Y. Lee, C.-M. Tseng, Y.-T. Lee, C.-K. Ni. Fluorescence spectroscopy of UV-MALDI matrices and implications of ionization mechanisms. *J. Chem. Phys.* **2014,** *141,* 164307.

[51] H.-Y. Lin, B. Song, I.-C. Lu, K.-T. Hsu, C.-Y. Liao, Y.-Y. Lee, C.-M. Tseng, Y.-T. Lee, C.-K. Ni. Is energy pooling necessary in ultraviolet matrix-assisted laser desorption/ionization? *Rapid Comm. Mass Spectrom.* **2014,** *28,* 77.

[52] F. H. Yassin, D. S. Marynick. Computational estimates of the gas-phase basicities, proton affinities and ionization potentials of the six isomers of dihydroxybenzoic acid. *Mol. Phys.* **2005,** *103,* 183.

[53] T. P. Lippa, S. N. Eustis, D. Wang, K. H. Bowen. Electrophilic properties of common MALDI matrix molecules. *Int. J. Mass Spectrom.* **2007,** *268,* 1.

[54] I.-C. Lu, K. Y. Chu, C.-Y. Lin, S.-Y. Wu, Y. A. Dyakov, C. J.-L., A. Gray-Weale, Y. T. Lee, C.-K. Ni. Ion-to-Neutral Ratios and Thermal Proton Transfer in Matrix-Assisted Laser Desorption/Ionization. *J. Am. Soc. Mass Spectrom.* **2015,**

[55] E. Stevenson, K. Breuker, R. Zenobi. Internal energies of analyte ions generated from different matrix-assisted desorption/ionization matrices. *J. Mass Spectrom.* **2000,** *35,* 1035.